Imaging blended VSP data using Full Wavefield Migration

Alok K. Soni and Eric Verschuur, Delft University of Technology*

SUMMARY

Blended source and/or simultaneous source acquisition for multi-offset and multi-azimuth VSP measurements can prove significantly beneficial in saving expensive borehole downtime. In the last few years, for the case of surface seismic data, it was proposed to redefine imaging and inversion of the blended data to handle the data directly without any need to separate the blended sources. Recently, we proposed the concept of full wavefield migration (FWM) to image VSP data, where using all the multiples - both surface and internal multiples - in the imaging provides better illumination, especially away from the well. Using the above mentioned two concepts, in this paper, we will show the potential of FWM to directly image blended VSP data, without the need for intermediate deblending. We can see FWM imaging as a deblending algorithm itself that transforms the blended data into the reflectivity image space by an inversion process. The concept of FWM formulated in terms of a constrained least-squares inversion scheme indeed enables us to use any kind of complex source wavefield to explain the subsurface reflectivity. The method is illustrated successfully for some synthetic blended VSP examples.

INTRODUCTION

Blended source and/or simultaneous source acquisition (Beasley et al., 1998; Ikelle, 2007; Berkhout, 2008; Neelamani et al., 2010) for surface seismic data is slowly becoming a routine practice in the oil and gas industry. Gulati et al. (2011) also proposed acquiring 3D VSP data using simultaneous sources to reduce the borehole acquisition cost significantly. Further, there has been been investigation in performing imaging (see Verschuur and Berkhout, 2009; Tang and Biondi, 2009; Jiang and Abma, 2010; Verschuur and Berkhout, 2011; Berkhout et al., 2012; Dai et al., 2012; Huang and Schuster, 2012) of the simultaneous or blended seismic data directly without separating the sources or deblending them.

For imaging VSP data, we recently proposed full wavefield migration (FWM) (for details on FWM concept and applications, please refer to Berkhout, 2012; Davydenko et al., 2012; Soni et al., 2012; Soni and Verschuur, 2013a,b). Using the full wavefield in imaging - i.e. including all multiple scattering - overcomes the limitation of poor illumination in VSP geometry case and, hence, FWM has the potential to be an important future imaging tool for VSP data.

In this paper, we will show the extension of using FWM to image blended VSP data and estimate the subsurface reflectivity, utilizing all the multiples, without a need for intermediate deblending. We approach the imaging as a constrained least-squares inversion process to estimate the true-amplitude angle-dependent reflectivity that explains the full (blended) wavefield. The constrained inversion helps in reducing the extrapolation artefacts and blending crosstalk and provides a high-resolution image of the reservoir. It is recursive in depth and incorporates the nonlinear reflection and transmission effects at each depth level, including internal multiples. In the next section, will discuss briefly the concept of full wavefield forward modelling for blended VSP data, after which the imaging process is described.

FULL WAVEFIELD MODELLING OF BLENDED VSP DATA

The full wavefield forward modelling of blended VSP data can be defined in similar way as described in Soni and Verschuur (2013a,b) for unblended VSP data. Lets assume a walkaway VSP geometry as shown schematically in the density or reflectivity model in Figure 1, where the sources are located at the surface, the receivers being located in the borehole.

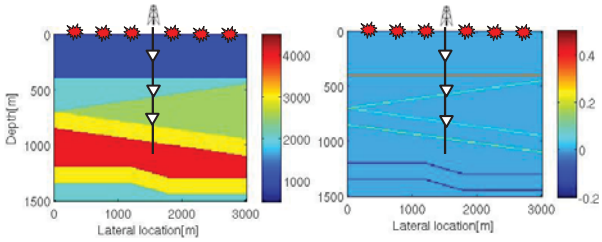

Figure 1: Synthetic a) density model and b) scalar reflectivity model used to illustrate the concept of full wavefield modelling and inversion for blended sources in a walkaway VSP geometry.

To start, we define the downward propagation operator to extrapolate the wavefield from a depth level z_{n-1} to a receiver in the borehole at depth level z_n and laterally located at x_r, which can be represented by a row vector $\vec{W}^{+\dagger}[(x_r,z_n),z_{n-1}]$ (note that row vectors are indicated by †). Similarly, the upward propagation operator to extrapolate the wavefield from a depth level z_{n+1} to a receiver at the same position can be represented by a row vector $\vec{W}^{-\dagger}[(x_r,z_n),z_{n+1}]$. Figure 2 schematically illustrates the downward and the upward propagation operators. Using the above-mentioned propagation operators, the downgoing wavefield element $P^{+}_{bl}(x_r,z_n)$ in the blended source acquisition at a receiver located in the borehole at depth z_n and laterally at x_r can be written as:

$$P^{+}_{bl}(x_r,z_n) = P^{+}_{dir,bl}(x_r,z_n) + \sum_{j=0}^{n-1} \vec{W}^{+\dagger}[(x_r,z_n),z_j][\delta\vec{P}(z_j)]_{bl}. \quad (1)$$

$P^{+}_{dir,bl}(x_r,z_n)$ is the direct wavefield element due to the blended source at the surface to a receiver in the borehole at depth z_n and laterally at x_r. Similarly, the upgoing wavefield element $P^{-}_{bl}(x_r,z_n)$ in the blended source acquisition at a receiver lo-

DOI http://dx.doi.org/10.1190/segam2013-0583.1

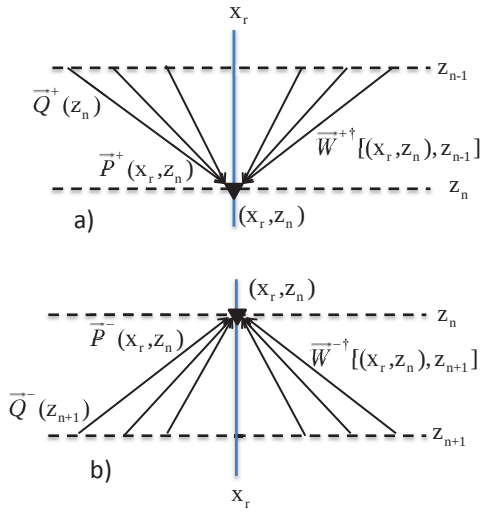

Figure 2: Schematic illustration of the a) downward propagation operator, row vector $\vec{W}^{+\dagger}[(x_r,z_n),z_{n-1}]$ and b) upward propagation operator, row vector $\vec{W}^{-\dagger}[(x_r,z_n),z_{n+1}]$.

cated in the borehole at depth z_n and laterally at x_r can be written as:

$$P^{-}_{bl}(x_r,z_n) = \sum_{j=n+1}^{N} \vec{W}^{-\dagger}[(x_r,z_n),z_j][\delta\vec{P}(z_j)]_{bl}. \qquad (2)$$

The two-way scattered wavefield $[\delta\vec{P}(z_n)]_{bl}$ due to blended sources for a horizontal depth level z_n can be written as:

$$[\delta\vec{P}(z_n)]_{bl} = \mathbf{R}^{\cup}(z_n)\vec{P}^{+}_{bl}(z_n) + \mathbf{R}^{\cap}(z_n)\vec{P}^{-}_{bl}(z_n), \qquad (3)$$

the matrices $\mathbf{R}^{\cup}(z_n)$ and $\mathbf{R}^{\cap}(z_n)$ represent reflectivity matrices related to the discontinuities at depth level z_n for the wavefield from above and below the layer, respectively. Please note that in the acoustic approximation, $\mathbf{R}^{\cap}(z_n) = -\mathbf{R}^{\cup}(z_n)$.

We can write the direct source wavefield incident from above, as observed at any horizontal depth level, i.e. $\vec{P}^{+}_{dir,bl}(z_n)$, due to a blended source wavefield at the surface, $\vec{S}^{+}_{bl}(z_0)$ as:

$$\vec{P}^{+}_{dir,bl}(z_n) = \mathbf{W}^{+}(z_n,z_0)\vec{S}^{+}_{bl}(z_0). \qquad (4)$$

Also, the direct source wavefield element $P^{+}_{dir,bl}(x_r,z_n)$ that is recorded or observed at a receiver located in the borehole at depth z_n and laterally at x_r can be written as

$$P^{+}_{dir,bl}(x_r,z_n) \quad = \vec{W}^{\dagger+}[(x_r,z_n),z_0]\vec{S}^{+}_{bl}(z_0). \qquad (5)$$

Here, the blended source vector $\vec{S}^{+}_{bl}(z_0)$ can be defined using the complete or full source matrix at the surface $\mathbf{S}(z_0)$ and a blending operator $\vec{\Gamma}_{bl}(z_0)$ (see Berkhout, 2008) as:

$$\vec{S}^{+}_{bl}(z_0) = \mathbf{S}^{+}(z_0)\vec{\Gamma}_{bl}(z_0), \qquad (6)$$

where the blending operator $\vec{\Gamma}_{bl}(z_0)$ can be written as $\vec{\Gamma}_{bl}(z_0) = [\gamma_1,\gamma_2,\gamma_3,.....,\gamma_N]$, with $\gamma_n = a_n e^{-j\omega T_n}$. In this case, T_n is a random time-shift applied to blend the sources and a_n is a scale factor that can be $a_n = 0$ for those sources not included in the blended experiment. We will use the term 'blending factor' to define the number of shots blended together in one experiment.

Figure 3 a, c, e, g show the direct downgoing wavefield as seen at a horizontal depth level 800m, due to a blended source experiment for blending factor one (no blending), two, three, and four, respectively. Similarly, Figure 3 b, d, f, h show the direct downgoing wavefield as received at the receivers in the borehole, due to a blended source experiment for blending factor one (no blending), two, three, and four, respectively.

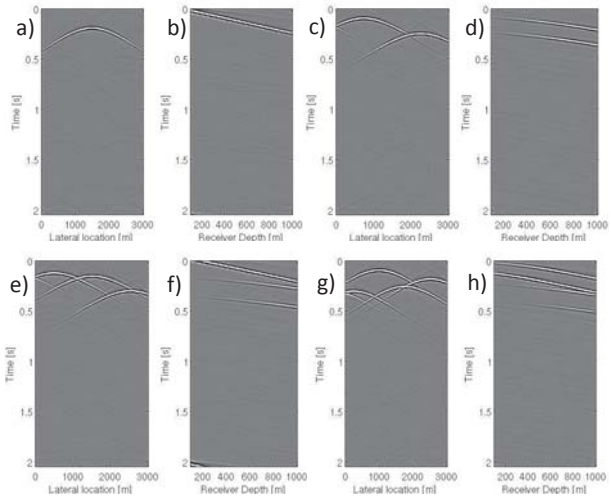

Figure 3: a), c), e) and g) show direct downgoing wavefield as seen at horizontal depth level 800m for a blended source experiment with blending factor one, two, three and four respectively. b), d), f) and h) show direct downgoing wavefield as received at receivers located in the borehole, for a blended source experiment with blending factor one, two, three and four respectively.

Similar as described in Berkhout (2012) and Soni and Verschuur (2013a,b), the full wavefield modelling includes iterative modelling of the upgoing and the downgoing wavefield as observed by the receivers location in the borehole, explained by Equations 1 and 2. Again, note that each iteration in the full wavefield modelling adds one higher order of scattering. To illustrate the full wavefield modelling for blended VSP data, we have used a dipping-layer density model as shown in Figure 1a and the corresponding reflectivity model as shown in Figure 1b. Figure 4, 5, 6 and 7 illustrate the full wavefield modelling for the blended data with blending factor three. Figure 4 shows an example common-shot gather modelled in the 1^{st} iteration, where 4a shows the downgoing direct source wavefield, 4b shows the upgoing reflection primaries-only wavefield and 4c shows the total wavefield, i.e. sum of the upgoing and the downgoing wavefield. Similarly, 5, 6 and 7 show an example modelled common-shot gather after 2^{nd}, 3^{rd} and 4^{th} iteration, respectively. Note that due to the blended sources, the wavefield becomes very complex even for this relatively simple subsurface model.

DOI http://dx.doi.org/10.1190/segam2013-0583.1

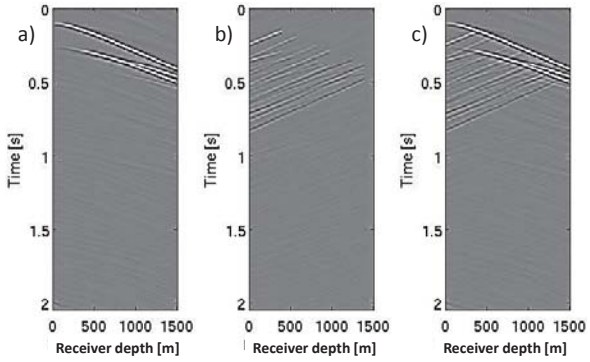

Figure 4: Iteration1: An example common-shot gather showing a) Downgoing, b) upgoing and c) total wavefield, for blending factor three.

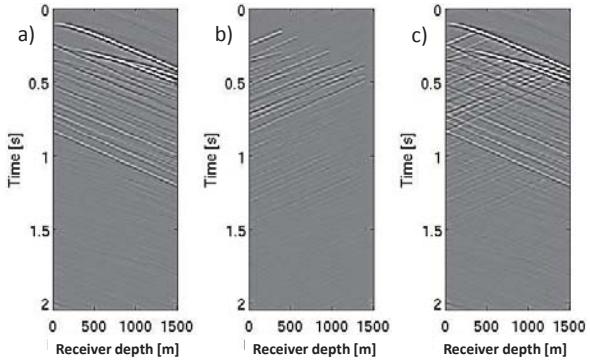

Figure 5: Iteration2: An example common-shot gather showing a) Downgoing, b) upgoing and c) total wavefield, for blending factor three.

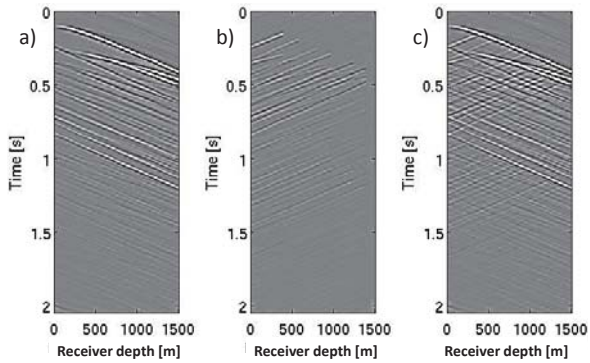

Figure 6: Iteration3: An example common-shot gather showing a) Downgoing, b) upgoing and c) total wavefield, for blending factor three.

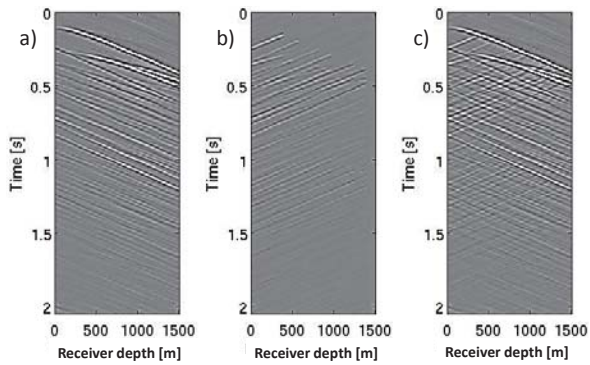

Figure 7: Iteration4: An example common-shot gather showing a) Downgoing, b) upgoing and c) total wavefield, for blending factor three.

FULL WAVEFIELD MIGRATION OF BLENDED VSP DATA: CONSTRAINED LEAST-SQUARES INVERSION

From the forward modelling formulation discussed in the previous section, we can write the estimate of the total wavefield recorded at one receiver location at depth z_n and laterally at x_r, as the sum of the upgoing and the downgoing wavefields as:

$$[P_{bl}(x_r,z_n)]_{est} = P^{+}_{bl}(x_r,z_n) + P^{-}_{bl}(x_r,z_n), \qquad (7)$$

which is a function of $[\delta\vec{P}(z_j)]_{bl}$ (see Equations 1 and 2) that contains the estimated reflectivity terms $\mathbf{R}^{\cap}_{est}(z_n)$ and $\mathbf{R}^{\cup}_{est}(z_n)$, and can be written as:

$$[\delta\vec{P}(z_n)]_{bl} = \mathbf{R}^{\cup}_{est}(z_n)\vec{P}^{+}_{bl}(z_n) + \mathbf{R}^{\cap}_{est}(z_n)\vec{P}^{-}_{bl}(z_n). \qquad (8)$$

Hence, we can formulate the estimation of the reflectivity at all depth levels as a constraint least-squares minimization problem, where the objective function to minimize becomes:

$$\begin{aligned} J &= \sum_{z_r}\sum_{\omega} ||[\vec{P}^{-}_{bl}(x_r,z_r)]_{obs} - [\vec{P}^{-}_{bl}(x_r,z_r)]_{est}||^2_2 \\ &+ \sum_{n}\sum_{j} log(1+R^2_{jj,n}/\sigma^2_r), \end{aligned} \qquad (9)$$

in which $R_{jj,n}$ is a sample of the reflectivity image (i.e. a diagonal element from matrix $\mathbf{R}(z_n)$) and σ_r is the weighting parameter in the Cauchy regularization term (Amundsen, 1991; Sacchi et al., 1998; Soni et al., 2012). We use the Cauchy norm as a constraint which tends to make the solution sparser and helps in reducing the extrapolation noise in VSP imaging as well as crosstalk due to the blended sources.

Note that the above mentioned objective function is meant for the data estimated at all receivers together, therefore, we have a sum over all z_r, i.e. receiver depths. We solve the above minimization problem to estimate the subsurface reflectivity using a conjugate gradient scheme (Hestenes and Stiefel, 1952).

To illustrate the FWM inversion scheme, we have modelled VSP data using an acoustic 2D finite-difference method, with a dense source geometry at the surface and using the density model as shown in Figure 1a. In order to test the imaging process for the blended data, we did the numerical blending by adding shots with random-time shifts, the number of shots added to make one blended shot is defined by the 'blending factor'. We have tested the scheme for blending factor one, two, three and four.

DOI http://dx.doi.org/10.1190/segam2013-0583.1

Figure 8 and 9 show example common shot and common receiver gathers after numerical blending, with blending factor one (equivalent to unblended data), two, three and four, respectively. Note that the blended data in the common receiver domain appears to be random, as expected, and the number of traces reduces with increasing blending factor. Also, note that the numerical blending leads to interference of the events in the common-shot domain.

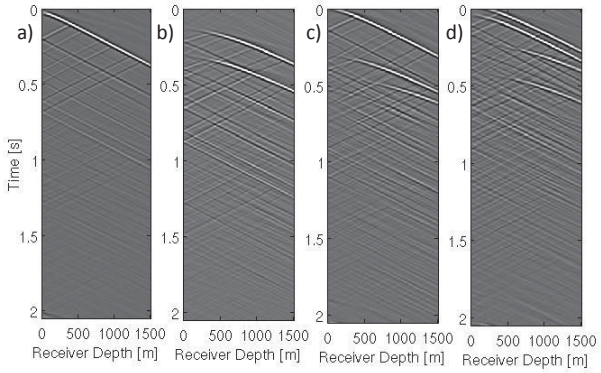

Figure 8: Examples of blended VSP data: a), b), c) and d) show an example common shot gather with blending factor = 1 (unblended data), 2, 3 and 4, respectively.

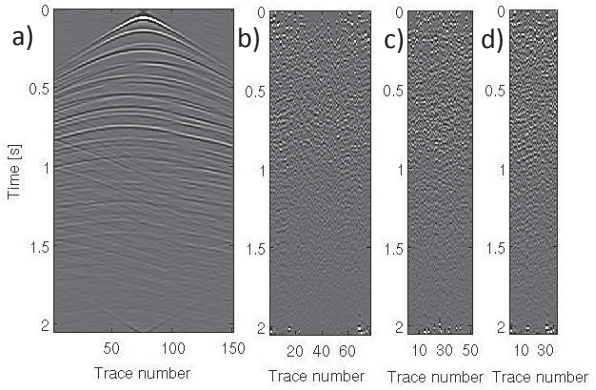

Figure 9: Examples of blended VSP data: a), b), c) and d) show an example common receiver gather with blending factor = 1 (unblended data), 2, 3 and 4, respectively.

Next, we perform FWM inversion on the blended data. Figure 10 show the images obtained after the 1^{st} (left column) and the 5^{th} iteration (right column) using the blended data with blending factor one, two, three and four. Note the illumination extent of the image is widened if we compare the images after the 1^{st} and 5^{th} iteration, as expected in FWM, because we use the full wavefield (including all multiples) to estimate the subsurface reflectivity. Again, each iteration explains one higher order of multiples in the data. The constrained least-squares inversion approach enables us to image the complex wavefield, without noticeable distortion from the blending process (compare Figure 10b with 10h)

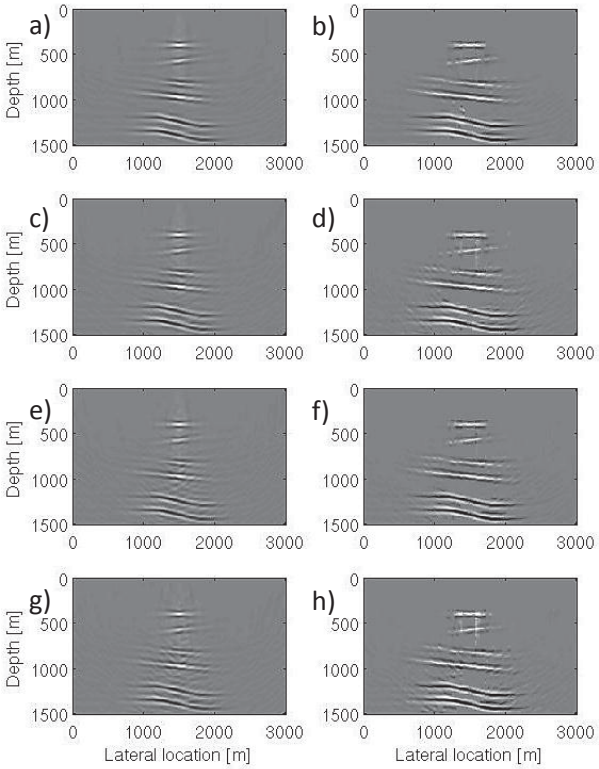

Figure 10: a), c), e) and g) Images after 1^{st} iteration for blending factor = 1, 2, 3 and 4 respectively. b), d), f) and h) Images after 5^{th} iteration for blending factor = 1, 2, 3 and 4 respectively.

CONCLUSIONS

Blended VSP acquisition can help in reducing the expensive rig-time or borehole acquisition time. Therefore, we expect to see more and more blended VSP acuisition in the future. In this paper, we demonstrated that FWM can be effectively used to directly image blended VSP data, i.e. utilizing the incoherent full wavefield due to the blended sources. We have shown simple synthetic examples to illustrate the imaging of blended VSP data with different blending factors. Clearly, from the imaging results, we can say that the constrained least-squares inversion scheme in FWM enables us to handle the blended data directly without any need of an intermediate deblending process. Furthermore, from the examples we see that the illumination extent of the image improves iteratively in FWM, utilizing all the multiples in the data. Finally, the cross-talk noise is very small because interference of wavefields in the blended source VSP data is suppressed by the least-squares inversion scheme.

ACKNOWLEDGMENTS

The authors thank the sponsoring companies of the Delphi consortium for their support.

DOI http://dx.doi.org/10.1190/segam2013-0583.1

http://dx.doi.org/10.1190/segam2013-0583.1

EDITED REFERENCES

Note: This reference list is a copy-edited version of the reference list submitted by the author. Reference lists for the 2013 SEG Technical Program Expanded Abstracts have been copy edited so that references provided with the online metadata for each paper will achieve a high degree of linking to cited sources that appear on the Web.

REFERENCES

Amundsen, L., 1991, Comparison of the least-squares criterion and the Cauchy criterion in frequency-wavenumber inversion: Geophysics, **56**, 2027–2035, http://dx.doi.org/10.1190/1.1443015.

Beasley, C. J., R. E. Chambers, and Z. Jiang, 1998, A new look at simultaneous sources: 68th Annual International Meeting, SEG, Expanded Abstracts, 133–135.

Berkhout, A. J., 2008, Changing the mindset in seismic acquisition: The Leading Edge, **27**, 924–938, http://dx.doi.org/10.1190/1.2954035.

Berkhout, A. J., 2012, Combining full wavefield migration and full waveform inversion: A glance into the future of seismic imaging: Geophysics, **77**, no. 2, S43–S50, http://dx.doi.org/10.1190/geo2011-0148.1.

Berkhout, A. J., D. J. Verschuur, and G. Blacquiere, 2012, Illumination properties and imaging promises of blended, multiple-scattering seismic data: A tutorial: Geophysical Prospecting, **60**, no. 4, 713–732, http://dx.doi.org/10.1111/j.1365-2478.2012.01081.x.

Dai, W., P. Fowler, and G. T. Schuster, 2012, Multi-source least-squares reverse time migration: Geophysical Prospecting, **60**, no. 4, 681–695, http://dx.doi.org/10.1111/j.1365-2478.2012.01092.x.

Davydenko, M., X. R. Staal, and D. J. Verschuur, 2012, Full wavefield migration in multidimensional media: Presented at the 82nd Annual International Meeting, SEG.

Gulati, J. S., A. Salama, S. W. Leaney, C. J. Beasley, E. Coste, H. Menkiti, and J. Tulett, 2011, Faster 3D VSP acquisition using simultaneous sources: 81st Annual International Meeting, SEG, Expanded Abstracts, 4249–4252.

Hestenes, M. R., and E. Stiefel, 1952, Methods of conjugate gradients for solving linear systems: Journal of Research of the National Bureau of Standards, **49**, no. 6, 409–436, http://dx.doi.org/10.6028/jres.049.044.

Huang, Y., and G. T. Schuster, 2012, Multisource least squares migration of marine streamer and land data with frequency-division encoding: Geophysical Prospecting, **60**, no. 4, 663–680, http://dx.doi.org/10.1111/j.1365-2478.2012.01086.x.

Ikelle, L. T., 2007, Coding and decoding: seismic data modeling, acquisition and processing: 77th Annual International Meeting, SEG, Expanded Abstracts, 66–70.

Jiang, Z., and R. Abma, 2010, An analysis on the simultaneous imaging of simultaneous source data: 80th Annual International Meeting, SEG, Expanded Abstracts, 3115–3119.

Neelamani, R., C. E. Krohn, J. R. Krebs, J. K. Romberg, M. Deffenbaugh, and J. E. Anderson, 2010, Efficient seismic forward modeling using simultaneous random sources and sparsity: Geophysics, **75**, no. 6, WB15–WB27, http://dx.doi.org/10.1190/1.3509470.

Sacchi, M. D., T. J. Ulrych, and C. J. Walker, 1998, Interpolation and extrapolation using a high-resolution discrete Fourier transform: IEEE Transactions on Signal Processing, **46**, no. 1, 31–38, http://dx.doi.org/10.1109/78.651165.

Soni, A. K., X. R. Staal, and D. J. Verschuur, 2012, VSP imaging using all multiples: Full wavefield migration approach: Presented at the 82nd Annual International Meeting, SEG.

Soni, A. K., and D. J. Verschuur, 2013a, Full wavefield migration of vertical seismic profiling data: Using all multiples for imaging away from the well: Presented at the Borehole Geophysics Workshop II, EAGE.

Soni, A. K., and D. J. Verschuur, 2013b, Imaging vertical seismic profiling data using full wavefield migration: Presented at the 75th Annual International Conference and Exhibition, EAGE.

Tang, Y., and B. Biondi, 2009, Least-squares migration/inversion of blended data: 79th Annual International Meeting, SEG, Expanded Abstracts, 2859–2863.

Verschuur, D. J., and A. J. Berkhout, 2009, Target-oriented, least-squares imaging of blended data: 79th Annual International Meeting, SEG, Expanded Abstracts, 2889–2893.

Verschuur, D. J., and A. J. Berkhout, 2011, Seismic migration of blended shot records with surface-related multiple scattering: Geophysics, **76**, no. 1, A7–A13. http://dx.doi.org/10.1190/1.3521658.